

Sidewinding on Slopes

Ross L. Hatton and Howie Choset
{rlhatton, choset}@cmu.edu

Abstract—Sidewinding is an efficient translation gait used by snakes over flat ground. When implemented on snake robots, it retains its general effectiveness, but becomes unstable on sloped surfaces. Flattening the sidewinding motion along the surface to provide a more stable base corrects for this instability, but degrades other performance characteristics, such as efficiency and handling of rough terrain. In this paper, we identify stability conditions for a sidewinder on a slope and find a solution for the minimum aspect ratio of the sidewinding pattern needed to maintain stability. Our theoretical results are supported by experiments on snake robots.

In constructing our stability analysis, we present a new, tread-based model for sidewinding that is both consistent with previous models and provides new intuition regarding the kinematics of the gait. This new interpretation of sidewinding further admits a symmetry-based model reduction that simplifies its analysis. Additionally, an intermediate stage of the theoretical work contains a comprehensive analysis of the behavior of an ellipse in rolling contact with a sloped surface.

I. INTRODUCTION

Snake robot locomotion has conventionally been approached from the perspective of finding efficient gaits to propel the robot over flat terrain or well-defined obstacles such as pipes, *e.g.* [1]–[5]. As these basic challenges come closer to being met, snake robots are emerging from laboratory settings and encountering less-structured environments. These new environments undermine some of the fundamental assumptions used in developing the basic gaits, prompting fresh analysis of how to increase their robustness to varying conditions.

Sidewinding provides a characteristic example of this situation. It is one of the most efficient locomotory gaits [5] and by many measures is robust, with its combination of looping coils and static ground contact points making it suitable for traversing a wide range of rocky, loose, or slippery terrain. Despite this robustness, our recent experience with outdoor snake robot operation has revealed a key weakness in past approaches to robotic sidewinding: when ascending slopes, the robot has a tendency to overbalance and roll downhill. While the basic solution to this problem, “flattening out” the sidewinding motion to provide a more stable base, is fairly straightforward and resembles the sidewinding motion of snakes on sand dunes, it comes with a cost. Depending on how it is accomplished, this change entails either reducing ground clearance and robustness over rocky terrain, or increasing the robot’s range of bending motion and thus the energy cost of the gait. A useful implementation of this principle, then, will take into account the magnitude of the slope and select an appropriate degree of flattening to

ensure stability on the slope while minimizing the reduction in robustness and efficiency.

This paper represents a first effort at characterizing the stability of a snake robot while sidewinding on uneven terrain. First, we present a new, reduced model of sidewinding. In this model the complex, three-dimensional motions of the gait are shown to be equivalent to the motion of a tread moving on the surface of an elliptical cylinder, which can be further simplified into a planar problem by taking advantage of the symmetry of the cylinder along its length. We then investigate the stability of a sidewinder on a sloped surface by identifying various margins of stability for the equivalent ellipse in contact with the slope. Finally, we verify these theoretical stability characteristics by comparing them against physical measurements taken on our snake robots.

II. BACKGROUND

Our analysis in this paper draws on prior research efforts regarding the motions of snakes and snake robots. While these are broad fields, the two developments which most contribute to the present work are the use of continuous backbone curves to represent snake robots and the kinematic description of snakes’ sidewinding gaits.

A. Backbone Curves

A powerful abstraction when working with snake robots is to step back from the specific characteristics of the robots and to work instead with a continuous *backbone curve* [6] describing the shape of the system. Doing so both simplifies the system representation, allowing access to the underlying physics of serpenoid motion, and makes the results of the analysis easily generalizable to snake robots of different morphologies. Once the system motions have been worked out, a fitting algorithm, such as those in Chirikjian and Burdick [6] and Andersson [7] for planar and universal-joint designs, or our formulation in [8] for alternating single-degree-of-freedom modules, can be applied to map the backbone curve into the specific joint angle commands needed to implement the motion.

B. Sidewinding

Sidewinding is an efficient translation gait that is especially effective when crossing loose or slippery ground. While the general mechanism of sidewinding was recognized in the seminal work of Mosauer [9] on ophidian locomotion, Burdick, Radford, and Chirikjian [10] were the first to study it in a rigorous mathematical fashion. Their analysis characterized the backbone shape during sidewinding as consisting

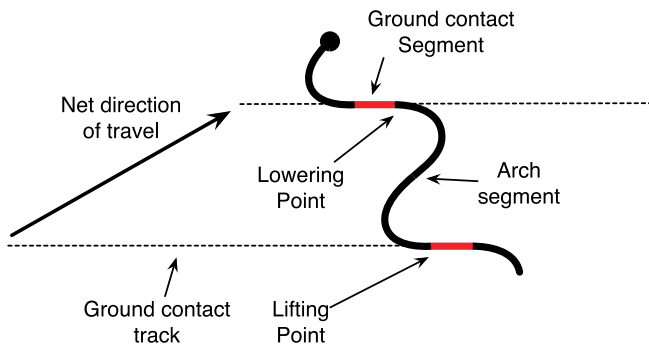


Fig. 1: Sidewinding motion. The ground contact segments are in static contact with the environment, while the arch segments are lifted from the ground and experience no friction. By progressively lifting the ground contact segments into arch segments while lowering arch segments down into ground contact segments, the snake or snake robot translates its body mass in the direction shown.

of *ground contact segments* and *arch segments*. The ground contact segments are parallel to each other and in static contact with the environment. The “S”-shaped arch segments connect the ground contact segments and are lifted from the ground. As illustrated in Fig. 1, the snake progressively raises one end of each ground contact segment into an arch segment, and lays down the arch segments into the other ends of the ground contacts. In doing so, the snake transfers its body mass between the *ground contact tracks*, producing a net displacement.

III. ANALYTICAL MODEL

For the majority of our analysis here, we use an elliptical-helix sidewinding model where the locus of the backbone curve in the xz plane is specified by a sine wave of amplitude a , and its height above the ground by a cosine wave of amplitude b , *i.e.*, its locus is

$$\begin{aligned} x &= a \sin(z + \omega\tau) \\ y &= b \cos(z + \omega\tau), \end{aligned} \quad (1)$$

where the $\omega\tau$ term phase-shifts the locus as the snake moves through the shapes of the gait. The ground contact segments appear at the low points of the cosine wave, which are collocated with linear stretches of the zx sine wave. Two factors recommend this backbone model as a basis for analysis. First, we have shown [8] that this backbone curve closely corresponds to the shape produced by snake robots executing sinusoid-based sidewinding, as in [2], [3], [5], [11], [12]. Second, the geometry of this backbone curve is well suited for analysis of its static, kinematic, and dynamic performance in sidewinding while incurring no loss of generality.

A. Reduced Model of Sidewinding

Sidewinding as described in Section II-B involves complex three-dimensional shape changes which both impede intuitive understanding and complicate analysis of the motion. To remedy this situation, we propose a reduced, planar model for sidewinding. This model is kinematically and dynamically equivalent to sidewinding from an external standpoint, but abstracts out the internal motions of the robot which are only necessary for control implementation.

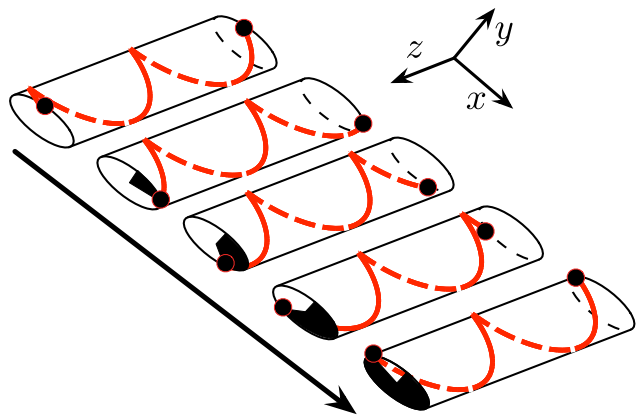


Fig. 2: The sidewinding backbone curve defined in (1) is an elliptical helix. As the backbone deforms over time, it acts as a helical tread around a hypothetical core cylinder, driving it forward.

The roots of this reduced model lie in Mosauer’s [9] likening of the sidewinding motion to the rolling of a circular helix such as a wire spring. In this analogy, the continuous laying down and peeling actions on either side of a ground contact segment correspond to the behavior of the standard rolling contact model, and the pitch of the helix means that it produces the same disconnected tracks at an angle to the direction of motion as does sidewinding. In fact, the sidewinding model defined in (1) defines such a rolling helix when $a = b$.

Mosauer’s observation provides a simplified frame of reference in which to consider sidewinding, but we must add a further refinement if we are to use it to generate a workable model. The rolling spring model accurately describes sidewinding when the backbone forms a circular helix, but becomes ambiguous when applied to other sidewinding backbone shapes, such as elliptical helices for which $a \neq b$. “Rolling” an elliptically shaped object has connotations of an “end-over-end” motion, in which the center of mass rises and falls as the contact point moves around the ellipse. As a better analogy for elliptical sidewinding, we present the “virtual tread” model illustrated in Fig. 2. In this interpretation of the gait, which was hinted at by Gray [13], we view the backbone as a helical tread moving around the (hypothetical) core elliptical cylinder, driving it forward. This tread model is easily extended to other sidewinding backbones by changing the shape of the core cylinder; *e.g.*, the ground contact segments can be extended by putting a flat on the bottom of the ellipse.

If the backbone helix contains at least two loops, it rests on a planar surface in the same manner as the full elliptical cylinder, and if it contains an integral number of loops, it has an equivalent radial mass distribution to the cylinder. For sidewinding backbones that meet these requirements, we can take advantage of the symmetry of the cylinder in the z direction and planarize the model, reducing sidewinding to the much simpler motion of an ellipse moving in the xy plane.

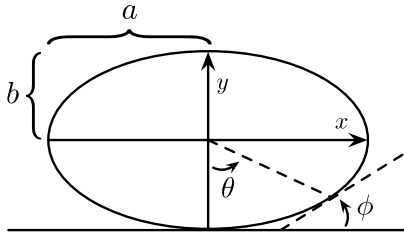


Fig. 3: An ellipse with semi-major axis a and semi-minor axis b . A tangent line with slope angle ϕ strikes the ellipse at polar angle θ , with $\tan \theta = \frac{a^2}{b^2} \tan \phi$.

B. Ellipse Contact Geometry

The stability of an ellipse on a sloped surface is dictated by the positioning of the center of mass of the ellipse relative to the point of contact with the ground. This positioning depends on the aspect ratio of the ellipse, the orientation of the ellipse, and the slope of the ground surface. To identify the relationship between these parameters and the center-of-mass position, we first find the polar angle θ from the minor axis at which a tangent line with slope ϕ strikes the ellipse, as in Fig. 3.

The ellipse in Fig. 3 is traced by the parameterized curve

$$\begin{aligned} x(t) &= a \sin t \\ y(t) &= -b \cos t, \end{aligned} \quad (2)$$

for $t = [-\pi, \pi]$. Note that the parameter t does not correspond directly to the polar angle θ , but that they are easily related. Starting with the property that $\tan \theta = -x/y$, substituting in x and y from (2) results in

$$\tan \theta = \frac{a}{b} \tan t. \quad (3)$$

Similarly, we can relate t to the tangent angle ϕ by noting that as $\tan \phi = dy/dx$ and

$$\frac{dx}{dt} = a \cos t \quad (4)$$

$$\frac{dy}{dt} = b \sin t, \quad (5)$$

dividing (5) by (4) gives the equality

$$\tan t = \frac{a}{b} \tan \phi. \quad (6)$$

Combining (3) with (6) provides the relationship between the polar and tangent angles,

$$\tan \theta = \frac{a^2}{b^2} \tan \phi. \quad (7)$$

From here, we can easily generalize to the case of finding the contact point between an ellipse with clockwise orientation α and an inclined surface with slope β , as in Fig. 4: because $\phi = \alpha + \beta$, the ellipse's contact with the surface is at

$$\theta = \arctan \left(\frac{a^2}{b^2} \tan (\alpha + \beta) \right). \quad (8)$$

Finally, we find the x and y positions of the center of mass relative to the contact point via the geometry illustrated in Fig. 5,

$$\begin{aligned} x_{\text{local}} &= -r(\theta) \sin (\theta - \alpha) \\ y_{\text{local}} &= r(\theta) \cos (\theta - \alpha), \end{aligned} \quad (9)$$

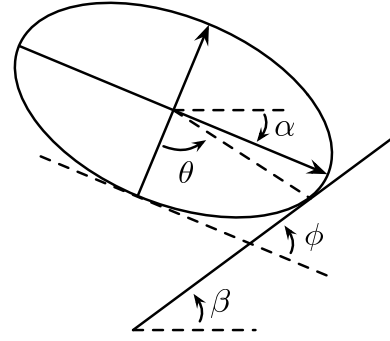


Fig. 4: Geometry of an ellipse with clockwise orientation α contacting an inclined angle with slope β .

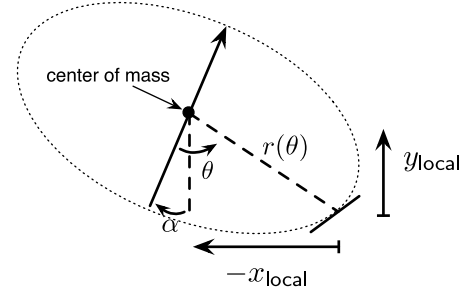


Fig. 5: Position of the center of mass of the ellipse relative to its contact point.

where r is the radius of the ellipse at θ ,

$$r(\theta) = \frac{ab}{\sqrt{a^2 \cos^2 \theta + b^2 \sin^2 \theta}}. \quad (10)$$

If the ellipse rolls along the surface without slipping, the distance traveled by the contact point is the signed distance along the perimeter of the ellipse from the minor axis to the contact point,

$$s(\theta) = \text{sign}(\theta) \cdot \int_0^\theta \sqrt{\left(\frac{dx}{d\vartheta}\right)^2 + \left(\frac{dy}{d\vartheta}\right)^2} d\vartheta. \quad (11)$$

IV. STABILITY

The fundamental requirement for effective sidewinding on a sloped surface is that the snake remain stable on the slope and not tumble down. A key factor in determining on how steep a slope a snake can sidewind is the aspect ratio of its backbone curve – intuitively, a backbone with a circular cross section will roll down even the gentlest slope, while one that flattens into a line will not roll at all.

A standard approach to determining the stability of an object is to compare the horizontal position of its center of mass to that of its contact footprint; the object is considered stable if the center of mass is inside the footprint, and unstable if it is outside. For example, the block on the left of Fig. 6 is stable, while the block on the right is not. We can also quantify the degree of stability, e.g., by considering either the maximum angular displacement that the object can sustain before becoming unstable, or the energy difference between this tipping point and the resting configuration.

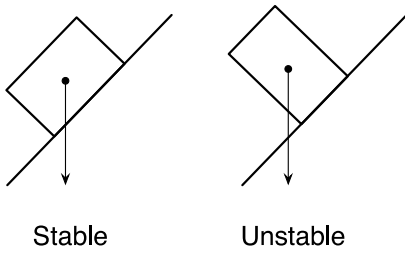


Fig. 6: At left, the block's center of mass is inside its footprint, and the block is correspondingly stable. At right, the block's center of mass is outside the footprint, making the block unstable.

A. Stable Configurations for Ellipses

Ellipses and other round objects generally have point contacts rather than contact footprints, but we can extend to them a similar notion of stability. We consider a stable resting configuration of such an object to be an equilibrium position in which the center of mass is directly above the contact point (for which gravity thus exerts no moment around the contact point) and for which small variations around the configuration are self correcting. More formally, an equilibrium angle on a slope β is one for which

$$x_{\text{local}}(\alpha, \beta) = 0 \quad (12)$$

and is a stable resting angle if the moment produced by small variations is self-correcting, *i.e.*,

$$\left. \frac{\partial x_{\text{local}}}{\partial \alpha} \right|_{\alpha} < 0, \quad (13)$$

and is an unstable equilibrium angle if

$$\left. \frac{\partial x_{\text{local}}}{\partial \alpha} \right|_{\alpha} > 0 \quad (14)$$

Figure 7(a) shows x_{local} as a function of the roll and slope angles for an ellipse with $a = 3$ and $b = 1$, along with its zero set. This zero set is the (α, β) locus of points satisfying (12), and has two identical sections offset by a roll angle of π , corresponding to the symmetry of the ellipse under rotations of half a revolution. Each of these sections is further divided into stable and unstable equilibria, according to the conditions in (13) and (14), respectively.

Alternatively, we can define the stable and unstable equilibria as the local extrema of the potential energy of the ellipse as it rolls along the slope. This potential energy is proportional to the height of the center of mass, y_{com} , which is in turn equal to the sum of y_{local} and the height of the ellipse's contact point with the slope. Applying the standard no-slip condition for rolling, the center of mass height is then

$$y_{\text{com}} = y_{\text{local}} + s(\theta(\alpha, \beta)) \sin \beta, \quad (15)$$

which is plotted in Fig. 7(b). As expected, the local minima and maxima of y_{com} with respect to α are collocated with the stable and unstable equilibria identified in Fig. 7(a), showing the two definitions of stability to be equivalent.

The equilibrium loci in Fig. 7 have critical points at a value of β that we term the *maximal stable slope* β_{max} , *i.e.* the greatest slope angle for which a resting angle exists for the given ellipse. For slopes steeper than this value, no

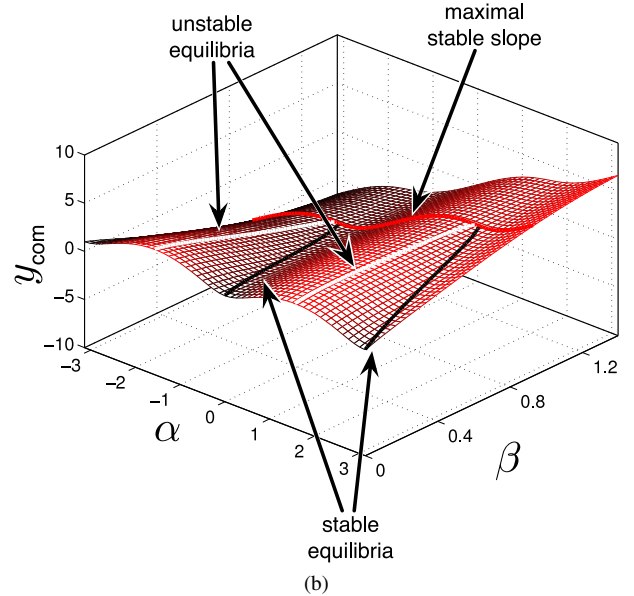
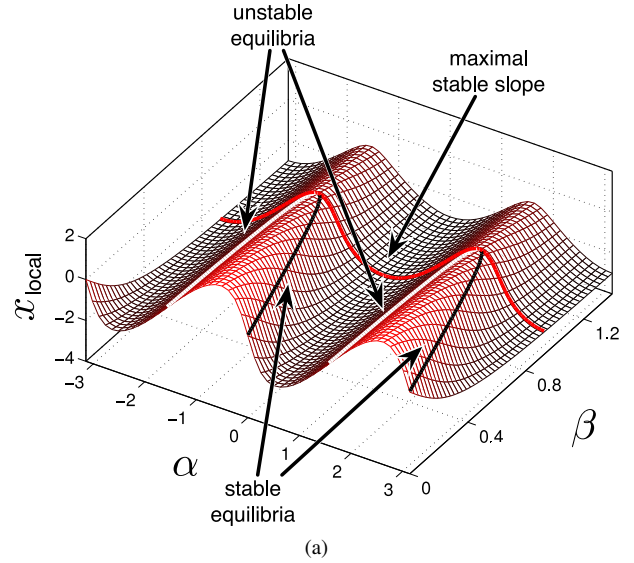


Fig. 7: The equilibria of an ellipse in contact with a slope can be regarded as either the zero set of $x_{\text{local}}(\alpha, \beta)$, or the local extrema of $y_{\text{com}}(\alpha, \beta)$. The stable equilibria have $\partial x_{\text{local}}/\partial \alpha < 0$, and are at the local minima of y_{com} with respect to α . For slopes steeper than the maximal stable slope, there are no equilibria and the ellipse cannot rest on the slope. The plots here correspond to an ellipse with $a = 3$ and $b = 1$.

configuration places the center of mass above the contact point, and the ellipse will always roll down.

B. Measuring the Stability

Having found the resting angles of the ellipse, we now turn our attention to measuring how stable these configurations are. Two convenient quantities for this purpose are the differences in α and y_{com} between the stable and unstable branches of the equilibrium locus, which we respectively term the *angular stability margin* and *energy stability margin*, as depicted in Fig. 8.

The unstable equilibria separate basins of attraction of the roll angle of the ellipse, so the angular stability margin serves to measure how much angular deviation is sustainable

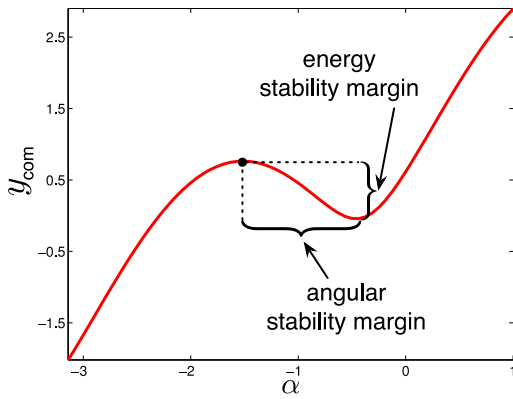


Fig. 8: Angular and energy stability margins for an ellipse with $a = 3$, $b = 1$ resting on a slope of angle $\beta = 0.4$ radians.

before the ellipse begins rolling towards a new resting angle. Similarly, the energy stability margin measures the energy disturbance that the ellipse can absorb without becoming unstable. These two quantities are plotted as functions of slope angle and ellipse aspect ratio in Fig. 9, where the zero-regions in the lower left corner represent combinations of a/b and β for which no resting angle exists. For the purposes of comparison in the energy metric, the ellipses of different aspect ratios are scaled to have unit perimeter. This preserves the length of the backbone curve and is thus consistent with the driving motivation of a tread model of sidewinding.

The shapes of the angular and energy margin functions in Fig. 9 yield some interesting comparisons. First, the angular margin is significantly more dependent on the slope angle than the aspect ratio, especially for $a/b > 2$, while the energy margin is approximately evenly dependent on both parameters. Second, the angular margin is convex, rising steeply from the null region before assuming a gentler slope, while the energy margin is concave, emerging smoothly from the null region, but growing more rapidly at smaller slope angles and larger aspect ratios.

We can gain additional insight on these two observations by fixing β and examining y_{com} as a function of α while varying a/b , as illustrated in Fig. 10(a), and by making the same examination for a fixed a/b and varying β , as in Fig. 10(b). As the aspect ratio increases in Fig. 10(a), the minima and maxima of y_{com} remain at approximately the same values of α , producing the cliff-like behavior of the angular margin in Fig. 9(a). In contrast, the minima and maxima of y_{com} smoothly emerge from the inflection point exhibited when $a/b = 1.5$, contributing to the smooth form of the energy margin in Fig. 9(b). In Fig. 10(b), increasing β reduces both the magnitude difference and the α -distance between the maxima and minima of y_{com} , generating the dependence on slope angle exhibited by both stability measures.

V. EXPERIMENTS

To verify our stability calculations, we formed snake robots from our laboratory into elliptical helices with a range of aspect ratios and placed them onto the high-friction inclined surface, shown in Fig. 11(a). By varying the slope of

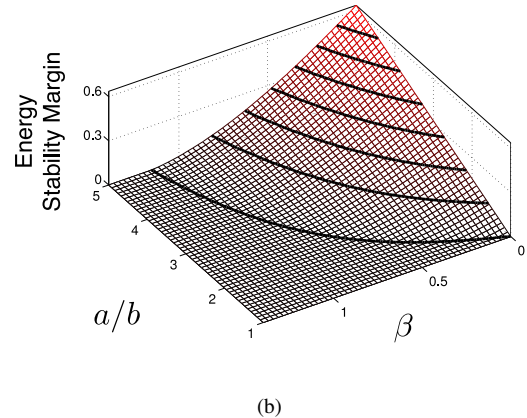
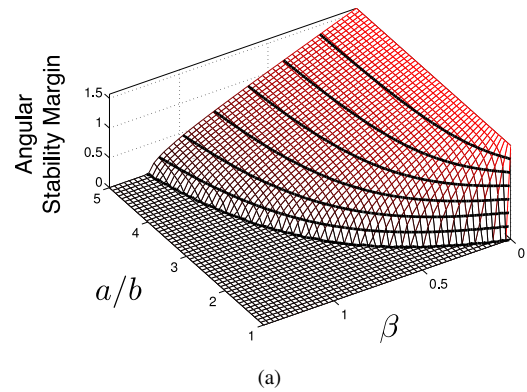


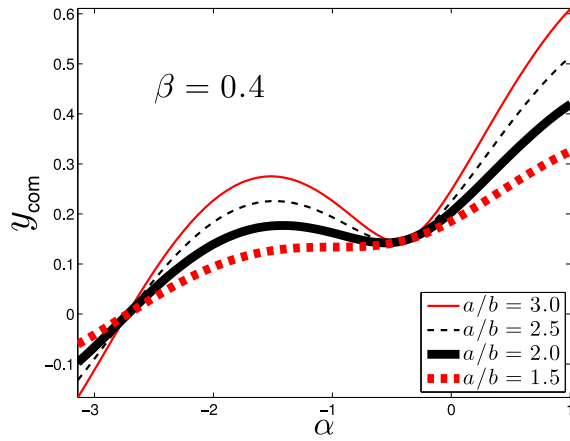
Fig. 9: The (a) angular and (b) energy stability margins for an ellipse resting on a slope, as functions of the slope angle and ellipse aspect ratio. The contour lines are evenly-spaced isoclines of the stability function.

the surface, we experimentally determined β_{max} as a function of the aspect ratio. As plotted in Fig. 11(b), the experimental and theoretical values for β_{max} agree quite strongly for the smaller aspect ratios. At the large end of the range, the results were truncated by $\tan(\beta_{max})$ exceeding the coefficient of friction between the robot and the surface; for these slopes, the robot slid before it tumbled.

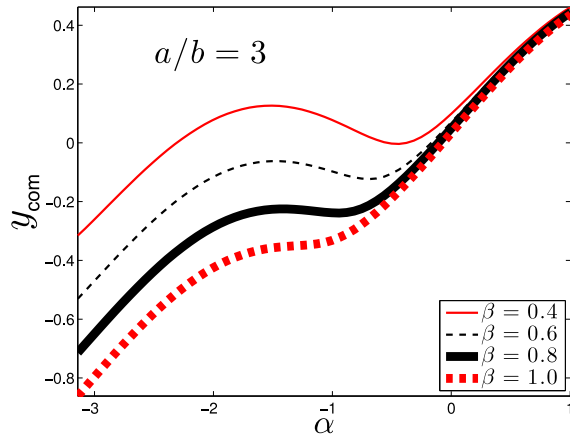
VI. CONCLUSIONS AND FUTURE WORK

The “virtual tread” model of sidewinding provides an intuitive perspective from which to consider this class of motion. Equally importantly from an analytical standpoint, it opens the door for a powerful planar reduction of the sidewinding model which greatly simplifies consideration of the stability of the gait. Using this model, we can use a simple geometric calculation to determine the minimum aspect ratio sidewinding backbone needed to maintain stability on a given slope.

This initial exploration of the model and the accompanying experiments suggest several avenues for continuing development of the model. We are especially interested in incorporating dynamic effects into the model; the similarity between our reduced sidewinding model and that of the dynamic rolling loop robot in [14] has not escaped us, and there is a strong potential for synergy in the analysis of the two systems. Other topics we will consider in our future work include analysis of the energy and mobility costs incurred by different aspect ratios; the benefits of using a different helix



(a)



(b)

Fig. 10: The center-of-mass height y_{com} as a function of roll angle α for (a) a slope of $\beta = 0.4$ and varying aspect ratio a/b and (b) for an aspect ratio of $a/b = 3$ and a varying slope angle β .

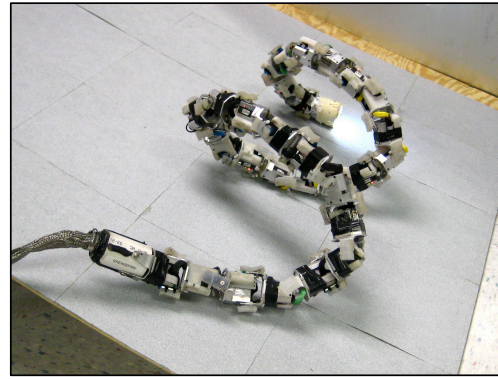
shape, such as one with an extended ground contact segment; and the effects of an unbalanced mass distribution, such as from a robot's tether or from a snake's keeping its head level while sidewinding with the rest of its body.

ACKNOWLEDGEMENTS

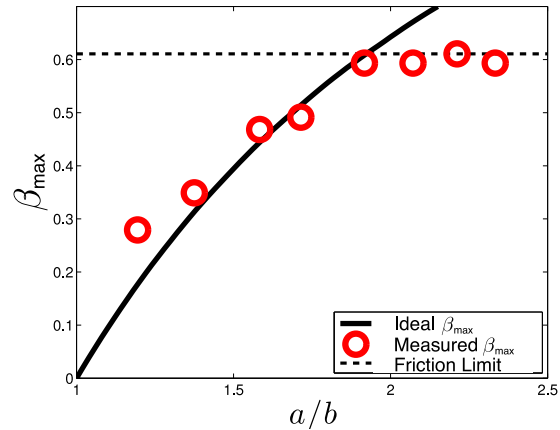
We would like to acknowledge the assistance of John Howland, Frederick C. Layton, Matthew Tesch, and Ben Morse with the experimental portion of this work.

REFERENCES

- [1] S. Hirose, *Biologically Inspired Robots (Snake-like Locomotor and Manipulator)*. Oxford University Press, 1993.
- [2] K. Lipkin, I. Brown, A. Peck, H. Choset, J. Rembisz, P. Gianfortoni, and A. Naaktgeboren, "Differentiable and Piecewise Differentiable Gaits for Snake Robots," in *Proceedings of IEEE/RSJ Intl. Conference on Intelligent Robots and Systems*, San Diego, CA, USA, Oct 29 - Nov 2 2007, pp. 1864–1869.
- [3] J. Gonzalez-Gomez, H. Zhang, E. Boemo, and J. Zhang, "Locomotion Capabilities of a Modular Robot with Eight Pitch-Yaw-Connecting Modules," in *9th International Conference on Climbing and Walking Robots.*, 2006.
- [4] A. J. Ijspeert and A. Crespi, "Online Trajectory Generation in an Amphibious Snake Robot Using a Lamprey-like Central Pattern Generator Model," in *IEEE Conference on Robotics and Automation*, 2007.
- [5] M. Tesch, K. Lipkin, I. Brown, R. Hatton, A. Peck, J. Rembisz, and H. Choset, "Parameterized and Scripted Gaits for Modular Snake Robots," *Advanced Robotics*, vol. 23, no. 9, pp. 1131–1158, 2009.



(a) Experimental apparatus. We formed the snake robot into an elliptical helix and placed it onto a high-friction inclined surface. By varying the aspect ratio of the helix and the slope of the surface, we experimentally determined β_{max} as a function of a/b .



(b) Experimental results. The friction limit is the slope for which $\tan(\beta_{\text{max}})$ exceeds the coefficient of friction between the robot and the surface, truncating the measurement of β_{max} .

Fig. 11: Experimental apparatus and results for measuring the maximal stable angle β_{max} as function of the aspect ratio a/b .

- [6] G. Chirikjian and J. Burdick, "Kinematics of Hyper-redundant Locomotion with Applications to Grasping," in *International Conference on Robotics and Automation*, 1991.
- [7] S. B. Andersson, "Discrete Approximations to Continuous Curves," in *IEEE International Conference on Robotics and Automation*, 2006.
- [8] R. L. Hatton and H. Choset, "Generating Gaits for Snake Robots by Annealed Chain Fitting and Keyframe Wave Extraction," in *IEEE/RSJ Int'l. Conf. on Intelligent Robots and Systems*, 2009.
- [9] W. Mosauer, "A Note on the Sidewinding Locomotion of Snakes," *The American Naturalist*, vol. 64, no. 691, pp. 179–183, March 1930.
- [10] J. Burdick, J. Radford, and G. Chirikjian, "A "Sidewinding" Locomotion Gait for Hyper-redundant Robots," *Robotics and Automation*, vol. 3, pp. 101–106, 1993.
- [11] J. Gonzalez-Gomez, H. Zhang, and E. Boemo, "Locomotion Principles of 1D Topology Pitch and Pitch-Yaw-Connecting Modular Robots," in *Bioinspiration and Robotics: Walking and Climbing Robots*. Advanced Robotics Systems International and I-Tech Education and Publishing, 2007.
- [12] S. Yu, S. Ma, B. Li, and Y. Wang, "Analysis of Helical Gait of a Snake-like Robot," in *Proceedings of the IEEE/ASME International Conference on Advanced Intelligent Mechatronics*, 2008.
- [13] J. Gray, "The Mechanism of Locomotion in Snakes," *Journal of Experimental Biology*, vol. 23, no. 2, pp. 101–123, December 1946.
- [14] J. Sastra, S. Chitta, and M. Yim, "Dynamic Rolling for a Modular Loop Robot," *International Journal of Robotics Research*, vol. 28, no. 6, pp. 758–773, 2009.